Daniel Marcos Bonotto. International Journal of Engineering Research and Applications
www.ijera.com
ISSN: 2248-9622, Vol. 15, Issue 9, September 2025, pp 94-103

RESEARCH ARTICLE OPEN ACCESS

Geochemical parameters for investigating the acid mine drainage (AMD) at Cerro Colorado, Rio Tinto Mines, Huelva, Spain

Daniel Marcos Bonotto
Geology Department, IGCE-Geosciences and Exact Sciences Institute, UNESP-São Paulo State University, Rio Claro, São Paulo State, Brazil
(Email: daniel.bonotto@unesp.br)

ABSTRACT
This paper describes a geochemical study of weathered rocky material and stream water samples collected at Cerro Colorado, Rio Tinto Mines, Spain. Geochemical analysis of the rocky material was done by X-ray fluorescence to obtain the concentration of major oxides SiO_2, TiO_2, Al_2O_3, Na_2O, K_2O, CaO, MgO, Fe_2O_3, MnO, and P_2O_5, as well as of the minor constituents ZrO_2, SrO, CuO, ZnO, BaO, Rb_2O, and Ga_2O_3. The stream water sample was analyzed by conventional techniques, such as potentiometry (pH and EC-electrical conductivity), methyl orange end-point titration (alkalinity), flame photometry (Na and K) and spectrophotometry (Ca, Mg, SiO_2, chloride, nitrate, and sulfate), whereas the determination of minor dissolved elements (Fe, Mn, Ni, Cu, Zn, As, Rb, Sr, Hg, Pb, and U) was done by the Total Reflection X-Ray Fluorescence Spectroscopy (TXRF). The analytical data were evaluated using geochemical diagrams, free software, and calculations involving the enrichment factor of the analyzed parameters.
Keywords **–** acid mine drainage, geochemical analysis, Cerro Colorado, Rio Tinto Mines

---

Date of Submission: 02-09-2025 Date of acceptance: 12-09-2025

I. Introduction

The largest volume of materials handled in the world corresponds to mine wastes. The generation of acidic drainage and the release of water containing high concentrations of dissolved metals from these wastes is an environmental problem of international scale. Acid mine drainage (AMD) is caused by the oxidation of sulfide minerals exposed to atmospheric oxygen. Although AMD is commonly associated with the extraction and processing of sulfide-bearing metalliferous ore deposits and sulfide-rich coal, AMD can occur wherever sulfide minerals are excavated and exposed to atmospheric oxygen [1].

Generally speaking, AMD refers to water discharged from active, inactive, or abandoned mines and reclaimed areas that have a relatively higher total acidity compared to total alkalinity, encompassing several chemical, biological, and electrochemical reactions [2]. Among the different AMD sources, there are construction rocks, diffuse seeps, tailings, open pit mines, stockpiles, and rock cuts/chips [2].

Extensive research on characterization, prediction, prevention, treatment, and control measures have been realized at least over the last 50 years, as acidic and metal-rich water presents a major threat to terrestrial and aquatic ecosystems, in addition to human health [3]. For instance, there are AMD reports focusing on several issues in various countries, including India, the USA, Canada, and South Africa [4-11].

In Brazil, multidisciplinary methods were applied to investigate the coal AMD occurring at Tubarão River, Santa Catarina State, Brazil, which included Raman spectroscopy, electron beam, and X-ray diffraction to study the minerals present in the sediment rivers close to that area, as well as ICP-MS (inductively coupled plasma mass spectrometry) for the elemental analysis of Al, As, Fe, K, Na, Ba, Mg, Mn, Ti, V, Zn, Ag, Co, Li, Mo, Ni, Se, Sn, W, B, Cr, Cu, Pb, and Sr, whose data were statistically treated by the PCA (Principal Component Analysis) method [12].

Another AMD area associated with coal mining activities in Brazil is located at Figueira City, Paraná State, here coded CMFC. Groundwater and surface waters from the Laranjinha River and the

Ribeirão das Pedras stream were monitored in two different seasons by [13], yielding the results summarized in Table 1. The AMD caused an increase in the concentration of some compounds in the groundwater samples, especially the high values of sulfate and iron, which modify the chemical equilibrium of the groundwater in both periods of collection [13]. When sulfide minerals are exposed to oxygen and water, an acid effluent is produced, promoting a sequence of reactions that lead to pH reduction and release of metals, such as iron and aluminum.

Table 1. Results of the analysis of surface waters (SW) and groundwater (GW) samples from the coal mining area at Figueira City (CMFC), Paraná State, Brazil, as reported by [13].

Parameter	Unit	SW Min.	SW Max.	GW Min.	GW Max.
pH	-	6.40	7.59	2.94	6.63
Conductivity	µS/cm	50	250	20	5500
SiO_2	mg/L	11.9	17.6	0.7	60.0
Na	mg/L	3.1	14.2	2.2	1009
K	mg/L	2.2	8.4	0.7	49.7
Ca	mg/L	0.6	22	0.4	240
Mg	mg/L	0.2	7.0	0.2	1400
Fe^{3+}	mg/L	0.01	0.41	0.05	988
Fe^{2+}	mg/L	<0.01	0.01	0.01	910
Ba	mg/L	1.5	4.7	1.5	285
Al	mg/L	0.04	12.5	1.3	4100
HCO_3^-	mg/L	18	60	10	860
Cl^-	mg/L	1.5	4.8	0.9	17.7
PO_4^{3-}	mg/L	0.2	1.6	0.01	5.2
SO_4^{2-}	mg/L	3	46	1.5	14400
NO_3^-	mg/L	1.5	3.5	0.5	580

Min.=minimum value; Max.=maximum value

The main mineral responsible for AMD generation is pyrite (FeS_2), whose oxidation by oxygen turns sulfur into sulfate, releasing ferrous iron (Fe^{2+}) and giving rise to 2 moles of acidity (H^+) for each mole of oxidized pyrite [14, 15]:

$$FeS_2 + 7/2\ O_2 + H_2O \rightarrow Fe^{2+} + 2\ SO_4^{2-} + 2\ H^+$$

Then, iron and other metals can react with alkali compounds, resulting in insoluble oxides/ hydroxides, or precipitates, in solution:

$$Fe^{2+} + 5/2\ H_2O + ½\ O_2 \rightarrow Fe(OH)_3\downarrow + 2\ H^+$$

Once the alkalinity available is depleted, metals can return to solution, increasing the Fe^{3+} concentration:

$$Fe^{2+} + 1/4\ O_2 + H^+ \rightarrow Fe^{3+} + 1/2\ H_2O$$

Such Fe^{3+} acts as an oxidizing agent to pyrite [16], characterizing a cyclical process that occurs until the ferric iron or pyrite becomes exhausted:

$$FeS_2 + 14\ Fe^{3+} + 8\ H_2O \rightarrow 15\ Fe^{2+} + 2\ SO_4^{2-} + 16\ H^+$$

The final product is iron in soluble (Fe^{2+}) or solid ($Fe(OH)_3$) forms. The Solubility of Fe3+ increases at low pH conditions, as well as its availability as an oxidizing agent, which is also influenced by the Eh, buffering capacity, and dissolved organic matter content in the solution [17].

One notorious AMD is that occurring for tens of kilometers at Rio Tinto in the Huelva Province, southwestern Spain, whose name means "stained river" in Spanish. Astrobiologists have been interested in the Rio Tinto and its surrounding area because the region's soils have similarities to those on Mars [18]. Iron- and potassium-rich sulfate mineral jarosite are common around the river and on Mars (the Red Planet), and because they contain signatures of bacterial activity at pH as low as 2, the astrobiologists from NASA have developed studies to evaluate how extremophiles live in and around the Rio Tinto may offer clues about how to search for evidence of life on Mars [18]. This paper describes a hydrogeochemical study focusing on that site, reporting a novel dataset and information obtained from the analysed samples.

II. Study area and sampling

Geologically, the mines located at the Rio Tinto area are inserted within the Iberian Pyrite Belt (IPB), which spans along a 230 km long by 50 km wide strip (about 8000 km^2 area) from southern Lisbon (Portugal) to the vicinity of Seville (Spain) [19]. The region also includes some of the largest accumulations of volcanogenic massive sulphide deposits in the Earth´s crust [20].

The IPB comprises three lithological groups from Devonian to Middle Carboniferous [21, 22]: (1) the Phyllite-Quartzite Group (PQ), formed by a sequence of shales and sandstones (thickness >2000m); (2) the Volcano-Sedimentary Complex (VSC), which overlies the PQ Group and includes a mafic-felsic sequence interstratified with shales; (3) the Culm Group, overlying the VSC, a turbidite sequence of shales, sandstones, and conglomerates.

Mineral resources estimates correspond to about 2000 Mt, with 1700 Mt being associated with massive sulphides and the remainder with stockwork-type mineralizations [20]. Evidence of mining exploitation in the region dates back over 5000 years, when the indigenous populace began to mine copper, but only from exposed outcroppings or from shallow depths [23]. Between 1800-1200 BCE,

silver minerals were extracted from oxidized sulphides, while by 1200-900 BCE, Iberian and Tartessian communities in the region exploited especially copper and tin, which are essential ingredients in bronze [23]. The Romans conquered the area in 206 BCE, and with their technologies, made large-scale mining possible, minting some of their first coins from the gold and silver extracted from the mines [23].

The mines were dug deeper with the advancement in tools and techniques, exposing more sulphides to air, water, and microorganisms that cause the Rio Tinto to blush and ever-deeper red. The Romans designed water wheels to remove water from deep underground mines [23]. After 200 years, the mines were no longer profitable, being left by the Romans to the new Iberian conquerors, Visigoths and Moors [23].

After a quiescent period during most of the Middle Ages, gold and silver exploration started again in the area in the 16th century, producing more than 10,000 tons of minerals per year by the end of the 18th century [23]. The increasing demand for copper, with its multiple uses in the electrical industry, in the early 19th century, favored mining activities in the area, also motivated by the chemical industry and the growing need for sulfuric acid for fertilizers, explosives, and other products [23].

All these developments, especially during the period 1850-2001, caused a drastic impact on the landscape. For instance, new smelters required significant amounts of wood, which led to the disappearance of the surrounding trees [24]. Also, calcinations utilization for the low-grade copper ores involved the 6-7 months roasting of 40-50 tons of ore in conical heaps to remove the sulphur, with the roasted ore being placed in tanks with acidic water to dissolve the copper; then, cementation produced copper in contact with iron scrap in channel systems [24]. Such calcination steps aggravated environmental and public health problems [24].

Currently, there are 7 operational mining centers at the IPB, which are giant (>50 Mt) and supergiant (>200 Mt) deposits [19, 25]: five in Spain (Las Cruces, Riotinto, Sotiel, Magdalena, and Aguas Teñidas), and two in Portugal (Aljustrel and Neves-Corvo). The average composition of known resources and reserves is 45% (S), 40% (Fe), 1.3% (Cu), 2% (Zn), 0.7% (Pb), 0.5 g/t (Au), 26 g/t (Ag), and concentrations ranging from tens to hundreds of ppm of minor metals such as Sn, Co, Cd, Hg, Bi, Sr, and In [26]. The largest individual polymetallic sulphide deposit (original reserves of 500 Mt sulphides) is the Riotinto orebody, consisting of three distinct mineralized zones (San Dionisio, San Antonio, and Cerro Colorado) that contain pyrite (FeS_2) with minor chalcopyrite ($CuFeS_2$), arsenopyrite (FeAsS), sphalerite (ZnS), and galena (PbS) covered by a weathering layer of gossans formed by an intense chemical weathering reaching up to 70 m thick [24].

The Rio Tinto headwaters are in the Sierra Morena, flowing to the port city of Huelva after an about 100-km course, where a 1.2 km long steel pier was built to aid in the rapid transfer of mined materials from iron horse to steam ship [23]. The Rio Tinto is a distinct case worldwide of acid drainage from sulphide, as the supergiant deposits in the area, the absence of country rocks with acid-neutralizing capacity, together with the intense mining exploitation, have caused extreme pH conditions and toxic concentrations of metals and metalloids from the headwaters to the mouth, not allowing that fish, amphibians, insects or plants live in their waters [24].

In this study, samples of surface water from a stream and weathered rocky material were collected during an excursion to Cerro Colorado mineralized zone, Rio Tinto Mines, Huelva, Spain, in February 2018 (Figs. 1-5).

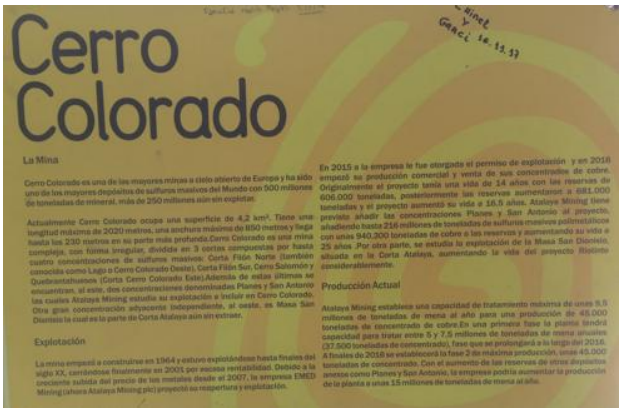

Fig. 1. Sign at the main entrance of Cerro Colorado mining area, Rio Tinto Mines, Huelva, Spain.

Fig. 2. Mining terraces, Cerro Colorado, Rio Tinto Mines, Huelva, Spain.

III. Experimental

One sample of each material collected was submitted to analysis conducted at IGCE-UNESP-Campus de Rio Claro. The weathered rocky material was analyzed by the X-ray fluorescence (XRF) technique, utilizing the pressed powder method and one WDXRF (wavelength dispersive X-ray fluorescence) spectrometer (Bruker S8 Tiger) that possesses rhodium anode, operates at 50 kV, 50 mA, and 1 kW of maximum voltage, current, and power, respectively, but without the need for external cooling. The basic operation concept consists of a source, the sample, and a detection system, as detailed by [27, 28].

Fig. 3. Exotic petrified tree trunks rising out of the soil close to a lake at Cerro Colorado, Rio Tinto Mines, Huelva, Spain.

Fig. 4. General view of a stream at Cerro Colorado, Rio Tinto Mines, Huelva, Spain, showing sulfurous yellow and orange at various stages of rust blend into blood red.

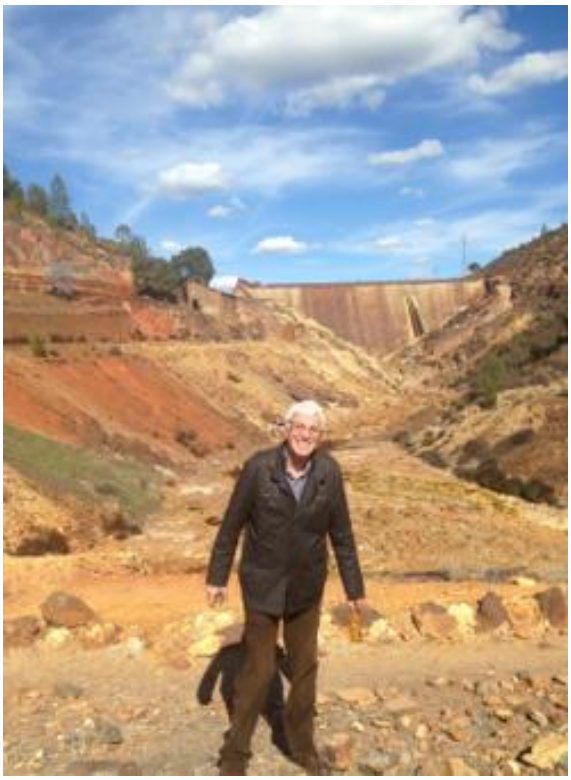

Fig. 5. Collection of a surface water sample from a stream at Cerro Colorado, Rio Tinto Mines, Huelva, Spain.

Fig. 6. Stream water sample from Cerro Colorado, Rio Tinto Mines, Huelva, Spain, submitted to chemical analysis.

Fig. 6 shows the typical yellow-orange-reddish color of the water sample analyzed, clearly pointing out the presence of dissolved iron. Standard analytical techniques, such as methyl orange end-point titration, potentiometry, and spectro-photometry, were used to obtain the parameters analyzed in the water sample as described by [29]. The pH measurement was performed by a digital portable meter (Digimed) coupled to a combination glass electrode (model KASVI), while the electrical conductivity (EC) was measured using a digital device (Analion, model C-702) coupled to a 1 cm^2 area Pt electrode calibrated with a KCl standard [29].

Alkalinity was measured by titration with 0.02 N sulfuric acid using the Hach 8221 - Buret Titration method [30]. Na and K were determined by the flame atomic emission spectrometry method, using a Benfer flame photometer (model BFC-300). Ca and Mg were determined by the colorimetric method (Hach Method 8030 - Calmagite Colorimetric) after chelating calcium with EGTA and Ca+Mg with EDTA [30].

Silica, chloride, nitrate, and sulfate in the water sample were also characterized by colorimetry utilizing the Hach DR/2700 spectrophotometer for every standardized Hach Method [30]: silica- Hach Method 8185 (Silicomolybdate); chloride- Hach Method 8113 (Mercuric Thiocyanate); nitrate- Hach Method 8039 (Cadmium reduction); sulfate- Hach Method 8051 (SulfaVer 4).

The determination of minor dissolved elements (Fe, Mn, Ni, Cu, Zn, As, Rb, Sr, Hg, Pb, and U) was done by the Total Reflection X-Ray Fluorescence Spectroscopy (TXRF) method, using a Bruker spectrometer, model S2 Picofox, and Yttrium as an internal standard. More details for such measurements are given by [31].

IV. Results and Discussion

The results obtained in all measurements are reported in Tables 2 and 3. The first aspect to be highlighted from analytical data is the acidic pH of the stream water sample (2.8), equivalent to the minimum value of 2.9 reported in Table 1 for groundwater occurring at the CMFC. Additionally, Table 3 shows that the dissolved sulfate and iron concentrations are high, as also typically reported for AMD elsewhere, including at the CMFC (Table 1).

Stosch [32] provided a free Excel template for plotting geochemical data in a diagram exhibiting the alkalis (A- Na_2O+K_2O), iron (F-FeO and Fe_2O_3), and magnesium (M-MgO) concentration, which was used to plot the dataset reported in Table 2, yielding the diagram shown in Fig. 7. The weathered rock material exhibits a tendency of alkalis enrichment compared to iron and magnesium.

Another useful tool to plot geochemical data is the ternary SiO_2-Al_2O_3-Fe_2O_3 diagram, in which the dataset reported in Table 2 was plotted, yielding the diagram shown in Fig. 8, which highlights the SiO_2-enrichment compared to Al_2O_3 and Fe_2O_3 in the weathered rocky material from Cerro Colorado.

Table 2. Results of the XRF measurements for the weathered rocky material from Cerro Colorado, Rio Tinto Mines, Huelva, Spain.

Parameter	Unit	Rio Tinto sample	Mean crustal concentration (Clarke)	FE1
SiO_2	%	69.30	43.92	1.12
TiO_2	%	0.24	0.68	0.35
Al_2O_3	%	13.36	15.1	0.88
Na_2O	%	2.96	3.2	0.92
K_2O	%	5.91	2.4	2.46
CaO	%	1.03	5.5	0.19
MgO	%	0.34	3.7	0.092
Fe_2O_3	%	4.44	6.28	0.71
MnO	%	0.05	0.1	0.50
P_2O_5	%	0.02	0.18	0.11
SO_3	%	2.02	-	-

ZrO_2	ppm	400	274.3	1.46
SrO	ppm	100	393.8	0.25
CuO	ppm	75	31.3	2.39
ZnO	ppm	100	81.2	1.24
BaO	ppm	1200	652	1.84
Rb_2O	ppm	200	170.7	1.17
Ga_2O_3	ppm	39	40.5	0.96

Table 3. Results of the analysis of the surface water sample collected at the stream occurring in Cerro Colorado, Rio Tinto Mines, Huelva, Spain.

Parameter	Unit	Rio Tinto sample	Mean concentration in freshwater	FE2
pH	-	2.8	-	-
EC	µS/cm	9,990	-	-
Na	mg/L	4,600	6.3	730.2
K	mg/L	23.46	2.3	10.2
Ca	mg/L	88	15	5.9
Mg	mg/L	2,940	4.1	717.1
SiO_2	mg/L	195	13.9	14
Bicarbonate	mg/L	<0.1	52	0.0019
Chloride	mg/L	0.9	7.8	0.12
Sulfate	mg/L	14,000	6.6	2,121.2
Nitrate	mg/L	600	1	600
Fe	mg/L	694.8	0.04	17,370.2
Mn	mg/L	68.5	0.007	9,786.1
Ni	mg/L	0.58	0.0003	1,943.3
Cu	mg/L	107.2	0.007	15,317.1
Zn	mg/L	133.7	0.02	6,684.2
As	mg/L	0.37	0.002	183
Rb	mg/L	0.044	0.001	44
Sr	mg/L	0.28	0.07	4.0
Hg	mg/L	0.043	0.00007	614.3
Pb	mg/L	0.23	0.001	231
U	mg/L	0.018	0.00004	450

Minetosh [33] developed a free online software to calculate the CIPW (Cross, Iddings, Pirsson, and Washington) NORM, i.e., the theoretical assemblage of minerals for a rock, based on the whole-rock chemical composition [34]. The software was utilized for the dataset reported in Table 2, yielding the following normative minerals for the weathered rocky material: quartz (35.23%), plagioclase (16.82%), orthoclase (35.87%), corundum (2.66%), hypersthene (0.85%), rutile (0.18%), ilmenite (0.11%), hematite (4.44%), apatite (0.05%), and zircon (0.07%). The dominant mineral phases (quartz and feldspars) may be related to rhyolites as source rocks in the study area [26].

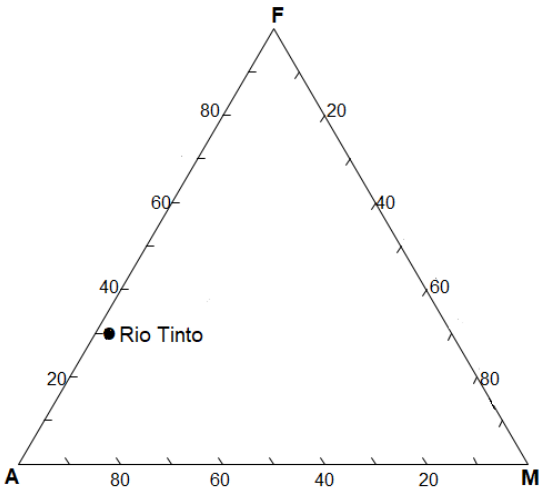

Fig. 7. AFM diagram plotting the geochemical data obtained for the weathered rocky material from Cerro Colorado, Rio Tinto Mines, Huelva, Spain.

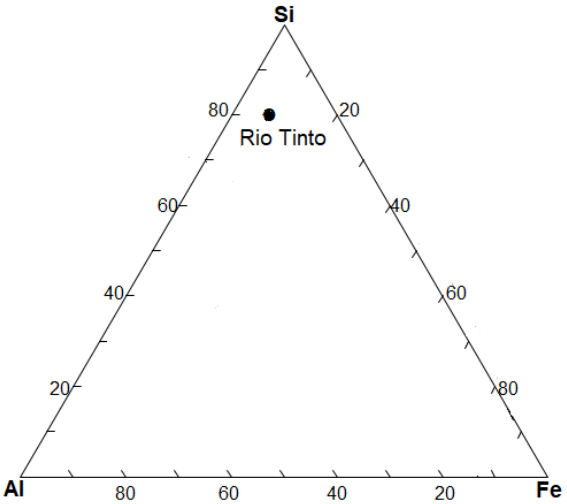

Fig. 8. SiO_2-Al_2O_3-Fe_2O_3 diagram plotting the geochemical data obtained for the weathered rocky material from Cerro Colorado, Rio Tinto Mines, Huelva, Spain.

Qualigraf software [35] allowed plotting the hydrochemical data of Table 3 in the Piper [36] and Schoeller [37] diagrams as shown in Figs. 9 and 10. In terms of dissolved cations, the stream water tends to be Mg-dominated, while it is chiefly sulfated, considering the dissolved anions.

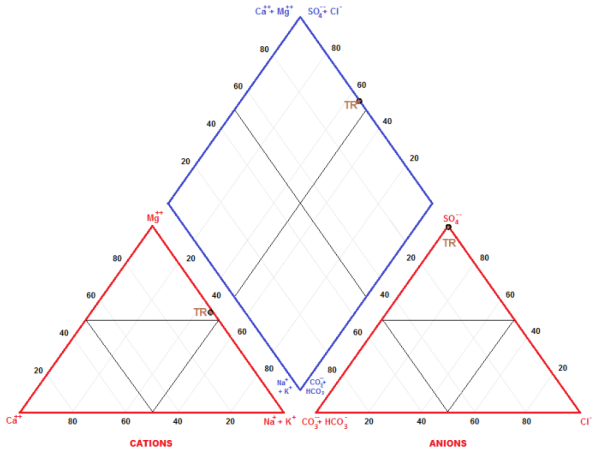

Fig. 9. Piper diagram plotting the hydrochemical data obtained for the stream water sample (TR) from Cerro Colorado, Rio Tinto Mines, Huelva, Spain.

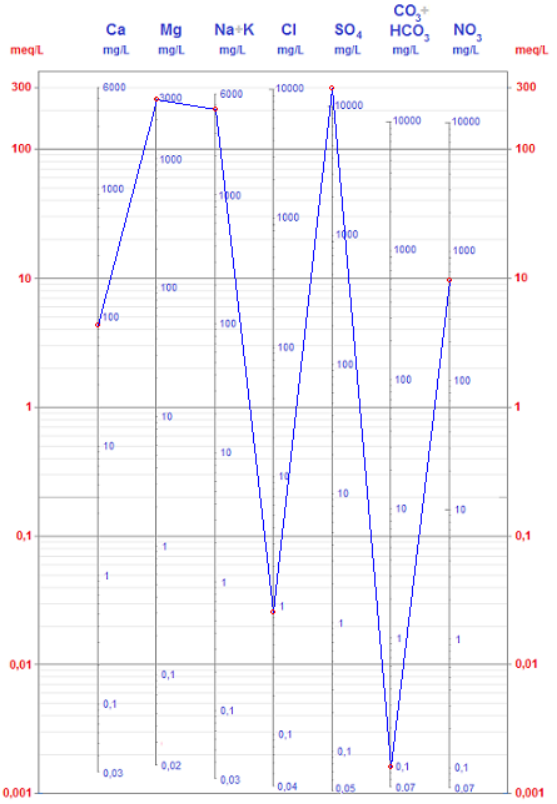

Fig. 10. Schoeller diagram plotting the hydrochemical data obtained for the stream water sample from Cerro Colorado, Rio Tinto Mines, Huelva, Spain.

The dataset reported in Table 2 was compared with the average crustal concentration, named Clarke, in honor of the American geochemist Frank W. Clarke, due to his extensive chemical analysis of rocks in the USGS from 1889 to 1924 [38]. Table 2 also shows the Clarke values of the constituents analyzed in this study as reported by [39], as well as the dimensionless enrichment factor (FE1) calculated by the ratio of the concentration of the constituent to its Clarke value.

The same concept of Clarke to crustal rocks has been applied by [40] to the hydrosphere, who suggested another dimensionless enrichment factor (FE2) calculated by the ratio of the concentration of the constituent in the water body to its Clarke value in the hydrosphere. Table 3 shows the Clarke values of the constituents analyzed in this study, as reported by [41], except for bicarbonate and sulfate, whose values are given by [42], and nitrate, which is reported by [43]. Table 3 also shows the dimensionless enrichment factor FE2.

The FE1 ratios reported in Table 2 indicate slight enrichment of the concentration in the weathered material to the Clarke for the following constituents: SiO_2, K_2O, ZrO_2, CuO, ZnO, BaO, and Rb_2O. Contrarily, there is an impoverishment in the remaining constituents, the most accentuated in MgO (FE1=0.092). The absence of high enrichment in metals often exploited in the studied area, like Fe, Cu, and Zn, is possibly related to the source rock type that yielded the weathered material, perhaps felsic epiclastic, and/or felsic volcanic/ volcanoclastic, instead of mineralized ore rocks containing pyrite, chalcopyrite, sphalerite, etc. [19].

Except for bicarbonate and chloride, the remaining FE2 ratios reported in Table 3 are above unity, between 4 (Sr) and 17,370 (Fe), indicating preferential occurrence of the constituents analyzed in the stream water in comparison with the global composition of the hydrosphere (fresh waters), which is a typical effect of the AMD.

Levels of bicarbonate corresponding to 860 mg/L in groundwater occurring at the CMFC (Table 1) allow for calculation FE2=16.5, revealing the lithological influence on the removal of constituents due to the AMD. Unlike in the Rio Tinto mining area, where FE2=0.0019, carbonate lenses have been described at the CMFC [44], whose dissolution is a bicarbonate source to the underground resources. The FE2 values for sulfate are close at the Rio Tinto (2,121) and CMFC (2,182) areas, but differ greatly for Fe, corresponding to 17,370 and 47,450, respectively.

It is also possible to suggest another dimensionless factor, preferential transfer (PT),

defined as PF=FE2/FE1, aiming to compare both enrichment factors, which indicates preferential migration of the constituent to the liquid phase if PT>1. Table 4 reports the calculated PT values from the available dataset (Tables 2 and 3), which range from 4 (K) to 24,465 (Fe), thus confirming the high iron transport to the liquid phase due to the effects of the AMD. Therefore, the factors FE1, FE2, and PT are helpful for the development of further investigations focusing on other sites affected by AMD occurring elsewhere.

Table 4. Preferential transfer (PT) of elements from analytical data obtained for samples collected at Cerro Colorado, Rio Tinto Mines, Huelva, Spain.

Element	PT	Element	PT	Element	PT
Na	794	Si	12.5	Cu	6,409
K	4	Fe	24,465	Zn	5,390
Ca	31	Mn	19,572	Rb	37.6
Mg	7,795	Sr	16		

V. Conclusion

The acid mine drainage (AMD) caused by the oxidation of sulfide minerals exposed to atmospheric oxygen is a large-scale environmental problem of international relevance. This process, accelerated by microbes, results in sulfuric acid and dissolved heavy metals like iron, which pollute surface and groundwater, contaminate ecosystems, and pose harmful effects on human health, animals, and plants. AMD occurs when sulfide minerals are excavated and exposed to atmospheric oxygen, although it is generally associated with the extraction and processing of sulfide-bearing metalliferous ore deposits and sulfide-rich coal. The Rio Tinto, Huelva, Spain, is a unique case worldwide of acid drainage from supergiant sulphide deposits, in which the absence of country rocks with acid-neutralizing capacity, coupled to intense exploitation, has caused extreme pH conditions and toxic concentrations of metals and metalloids that favored life conditions only for microorganisms and certain algae species. The stream water analyzed from Cerro Colorado, Rio Tinto Mines, is very acidic (pH=2.8), Mg-dominated and chiefly sulfated, possessing an elevated dissolved iron concentration of almost 700 mg/L, which are typical conditions of waters affected by AMD. A proposed dimensionless factor, named preferential transfer (PT), pointed out a high value of 24,465 for Fe, confirming its accentuated migration to the liquid phase due to the effects of the AMD, thus showing the PT usefulness to study other sites affected by AMD worldwide.

Acknowledgements

CNPq (Brazilian National Council for Scientific and Technological Development) for Grant No. 304010/2021-9. Gabrielle R. Ceccato and Fábio O. Thomazini for chemical analysis of the samples.

REFERENCES

[1] D.W. Blowes, C.J. Ptacek, J.L. Jambor, and C.G. Weisener, The geochemistry of acid mine drainage, in H.D. Holland, and K.K. Turekian (Eds.) *Treatise on Geochemistry*, v. 9 (Amsterdam: Elsevier, 2003), 149-204.

[2] B.S. Acharya, and G. Kharel, Acid mine drainage from coal mining in the United States – An overview, *Journal of Hydrology*, 588, 2020, e125061.

[3] R. Verburg, N. Bezuidenhout, T. Chatwin, and K. Ferguson, The global acid rock drainage guide (GARD Guide), *Mine Water Environment*, *28* (4), 2009, 305.

[4] S.M. Equeenuddin, S. Tripathy, P.K. Sahoo, and M.K. Panigrahi, Hydrogeochemical characteristics of acid mine drainage and water pollution at Makum Coalfield, India, *Journal of Geochemical Exploration*, *105* (3), 2010, 75-82.

[5] S. Swer, and O.P. Singh, Status of water quality in coal mining areas of Meghalaya, India, *Proc. National Seminar on Environmental Engineering with special emphasis on Mining Environment*, NSEEME-2004, 2004, 19-20.

[6] R.K. Tiwary, Environmental impact of coal mining on water regime and its management, *Water, Air, & Soil Pollution, 132* (1-2), 2001, 185-199.

[7] G.A. Brodie, D.A. Hammer, and D.A. Tomljanovich, Constructed wetlands for acid drainage control in the Tennessee Valley: Mine drainage and surface mine reclamation, *US Bureau of Mines Information Circular*, *9183*, 1988, 325-331.

[8] J.G. Skousen, P.F. Ziemkiewicz, and L.M. McDonald, Acid mine drainage formation, control and treatment, *Extractive Industries and Society*, *6* (1), 2019, 241-249.

[9] M. Ramasamy, and C. Power, Evolution of acid mine drainage from a coal waste rock pile reclaimed with a simple soil cover, *Hydrology*, *6* (4), 2019, e83.

[10] S. Geldenhuis, and F.G. Bell, Acid mine drainage at a coal mine in the eastern Transvaal, South Africa, *Environmental Geology*, *34* (2-3), 1998, 234-242.

[11] G.M. Ochieng, E.S. Seanego, and O.I. Nkwonta, Impacts of mining on water resources in South Africa: A review, *Scientific Research and Essays*, *22*, 2017, 3351-3357.

[12] L.F.O. Silva, S.F.-O. de Vallejuelo, I. Martinez-Arkarazo, K. Castro, M.L.S. Oliveira, C.H. Sampaio, I.A.S. de Brum, F.B.de Leão, S.R. Taffarel, and J.M. Madariaga, Study of environmental pollution and mineralogical characterization of sediment rivers from Brazilian coal mining acid drainage, *Science of the Total Environment*, *447*, 2013, 169-178.

[13] J.A. Galhardi, and D.M. Bonotto, Hydrogeochemical features of surface water and groundwater contaminated with acid mine drainage (AMD) in coal mining areas: A case study in southern Brazil, *Environmental Science and Pollution Research*, *23*, 2016, 18911-18927.

[14] A. Al-Hasimi, G.J. Evans, and B. Cox, Aspects of the permanent storage of uranium tailings, *Water, Air, & Soil Pollution, 88*, 1996, 83-92.

[15] A. Akcil, and S. Koldas, Acid Mine Drainage (AMD): Causes, treatment and case studies, *Journal of Cleaner Production*, *14* (12-13), 2006, 1139-1145.

[16] B. Lottermoser, *Mine wastes: Characterization, treatment and environmental impacts*, 3rd edn. (Springer, Berlin, 2010).

[17] K. Küsel, Microbial cycling of iron and sulfur in acid coal mining lake sediments, *Water, Air, & Soil Pollution, 3*, 2003, 67-90.

[18] NASA Earth Observatory, *Spain's Stained River*. [https://earthobservatory.nasa.gov/images/147459/spains-stained-river] Accessed 7 September 2025.

[19] R. Sáez, F. González, T. Donaire, M. Toscano, L. Yesares, G.R. de Almodóvar, and C. Moreno, Updating geological information about the metallogenesis of the Iberian Pyrite Belt, *Minerals*, *14*, 2024, e860.

[20] J.M. Leistel, E. Marcoux, D. Thieblemont, C. Quesada, A. Sánchez, G.R. Almodóvar, E. Pascual, and R. Sáez, The volcanic-hosted massive sulphide deposits of the Iberian Pyrite Belt: Review and preface to the special issue, *Mineralium Deposita*, *33*, 1998, 2-30.

[21] N.G. Adamides, Rio Tinto (Iberian Pyrite Belt): A world-class mineral field reopens, *Applied Earth Sciences*, *122*, 2013, 1-15.

[22] F. Tornos, Environment of formation and styles of volcanogenic massive sulfides: The Iberian Pyrite Belt, *Ore Geology Reviews*, *28*, 2006, 259-307.

[23] Natural History, *Rio Tinto and the Mines*. [https://www.naturalhistorymag.com/perspectives/013198/rio-tinto-and-the-mines] Accessed 7 September 2025.

[24] M. Olias, and J.M. Nieto, Background conditions and mining pollution throughout history in the Rio Tinto (SW Spain), *Environments*, *2* (3), 2015, 295-316.

[25] R. Sáez, E. Pascual, M. Toscano, and G.R. Almodóvar, The Iberian type of volcano-sedimentary sulphide deposits, *Mineralium Deposita*, *34*, 1999, 549-570.

[26] F.J.A.S. Barriga, D. de Carvalho, and A. Ribeiro, Introduction to the Iberian Pyrite Belt, in F.J.A.S. Barriga, and D. de Carvalho (Eds.) *Geology and VMS Deposits of the Iberian Pyrite Belt*, (SEG Neves Corvo Field Conference: SEG-Society of Economic Geologists, 1997) Guidebook Series v. 27, 1-20.

[27] D.M. Bonotto, and G. Roveratti, Comparative geochemical analysis by XRF of sediments for limnological studies, in B. Veress, and J. Szigethy (Eds.) *Horizons in Earth Sciences Research,* v. 20 (New York, USA: Nova Science, 2020), 41-64.

[28] G. Roveratti, and D.M. Bonotto, End-user procedure for the calibration of an X-rays fluorescence spectrometer, in J.C. Taylor (Ed.) *Advances in Chemistry Research* (New York, USA: Nova Science, 2017), 231-247.

[29] D.M. Bonotto, M. Lunardi, and A. Goonetilleke, Hydrochemistry of blackwaters in a shoreline zone of São Paulo State, Brazil, *Journal of Marine Science and Engineering*, *13*, 2025, e1575.

[30] Hach, *Water analysis handbook*, 4th edn. (Hach Company, Loveland, 2000).

[31] D.M. Bonotto, and G. Roveratti, Hydrochemical analysis of groundwater from Brazilian aquifers by TXRF analysis, in H. Bailey (Ed.) *Aquifers: Properties, roles and research* (New York, USA: Nova Science, 2017), 57-79.

[32] H.G. Stosch, *TAS diagram, K_2O-SiO_2 diagram and AFM diagram template for Excel*. [https://zenodo.org/records/5977826] Accessed 30 August 2025.

[33] Minetosh online, *CPIW-norm calculation*. [https://minetoshsoft.com/cipw/cipwcalc.html] Accessed 30 August 2025.
[34] S. Dutch, *The CIPW Norm*. [https:// academic.sun.ac.za/natural/geology/undergraduate/G314/G314-06-Prac2-Calculating%20CIPW%20 norms.pdf] Accessed 30 August 2025.
[35] Funceme (Foundation of Ceará State for Meteorology and Hydric Resources), *Qualigraf*. [https://qualigraf.funceme.br/] Accessed 7 September 2025. (in Portuguese)
[36] A.M.A. Piper, A graphic procedure in the geochemical interpretation of water analyses, *Transactions of the American Geophysical Union, 25*, 1944, 914-928.
[37] H. Schoeller, *Groundwaters*. (Masson & Cie, Paris, 1962). (in French)
[38] N. Charles, G. Lefebvre, R. Tuloup, A. Carreaud, A. Boubault, A.-S. Serrand, M. Picault, V. Piguet, V. Manzin, F. Deswarte, and J. Aupoil, Mineral resource abundance: An assessment methodology for a responsible use of mineral raw materials in downstream industries, *Sustainability*, *15*, 2023, e16783.
[39] K.H. Wedepohl, The composition of the continental crust, *Geochimica et Cosmochimica Acta*, *59* (7), 1995, 1217-1232.
[40] A. Ryskeldieva, D. Burlibaeva, A. Yerdesbay, G. Kamelkhan, and N. Sarova, Clarkeconcentrations of heavy metals in surface waters of the transboundary river Yertis (Kazakhstan), *Water Science*, *37* (1), 2023, 18-27.
[41] S.R. Taylor, and S.M. McLennan, *The continental crust: Its composition and evolution*, (Blackwell Scientific Publ., Oxford, 1985).
[42] E.K. Berner, and R.A. Berner, *The global water cycle*, (Prentice-Hall, Englewood Cliffs, NJ, 1987).
[43] R.E. Turner, N.N. Rabalais, D. Justic, and Q. Dortch, Global patterns of dissolved N, P and Si in large rivers, *Biogeochemistry*, *64*, 2003, 297-317.
[44] V.P. Campaner, W. Luiz-Silva, and W. Machado, Geochemistry of acid mine drainage from a coal mining area and processes controlling metal attenuation in stream waters, southern Brazil, *Anais da Academia Brasileira de Ciências*, *86* (2), 2014, 539-554.